

Magnetization steps and cluster-type statistics for a diluted Heisenberg antiferromagnet on the square lattice: Models with two exchange constants

Yaacov Shapira*

Department of Physics and Astronomy, Tufts University, Medford, MA 02155

Valdir Bindilatti†

*Instituto de Física, Universidade de São Paulo,
Caixa Postal 66.318, 05315-970 São Paulo-SP, Brazil*

(Dated: August 28, 2018)

Magnetization steps (MST's) from a strongly diluted antiferromagnet on the square lattice are discussed theoretically. Thermal equilibrium, at temperature T and magnetic field B , is assumed. Two specific cluster models with the largest and second-largest exchange constants, $J^{(1)}$ and $J^{(2)}$, respectively, are considered in detail. In the J_1 - J_2 model, $J^{(1)}$ is the nearest-neighbor (NN) exchange constant J_1 , and $J^{(2)}$ is the second-neighbor exchange constant J_2 . In the J_1 - J_3 model, $J^{(1)}=J_1$, and $J^{(2)}$ is the third-neighbor exchange constant J_3 . For these two models, all cluster types of sizes $n_c \leq 5$ are identified, and their statistics is expressed using perimeter polynomials for cluster types. All cluster types with sizes $n_c > 1$ give rise to MST's. Calculated curves of the isothermal magnetization M as a function of B are given for widely different ratios $J^{(2)}/J^{(1)}$. Some of the information contained in these magnetization curves is conveyed more directly by the derivative curves, dM/dB versus B . The series of peaks in the derivative curve is called the "MST spectrum." This spectrum is much simpler when the ratio $J^{(2)}/J^{(1)}$ is very small. A detailed discussion of the exchange-bond structure and MST spectra for cluster models with a very small ratio $J^{(2)}/J^{(1)}$ is given in the following paper. The "parent" models of the J_1 - J_2 model are the J_1 and J_2 models. For the J_1 - J_3 model the parent models are the J_1 and J_3 models. Relations between the J_1 - J_2 and the J_1 - J_3 models and their respective parent models are discussed. The three parent cluster models (J_1 -, J_2 -, and J_3 -models) are identical, except for the neighbor associated with the one exchange constant J that is included in the model. Common properties of such "isomorphic" cluster models are discussed.

PACS numbers: 05.50.+q, 75.50.Ee, 71.70.Gm, 75.10.Jm, 75.10.Nr, 75.60.Ej

I. INTRODUCTION

An earlier theoretical paper¹ (hereafter I) on magnetization steps from a diluted Heisenberg antiferromagnet on the square lattice was largely devoted to the nearest-neighbor (NN) cluster model. To obtain magnetization steps (MST's), the NN exchange constant J_1 must be antiferromagnetic (AF). The present paper discusses cluster models with two exchange constants: the largest, called $J^{(1)}$, and the second-largest, $J^{(2)}$. Both exchange constants are assumed to be AF.

Some of the discussion in the present paper applies to any $J^{(1)}$ - $J^{(2)}$ cluster model, regardless of the neighbors associated with $J^{(1)}$ and $J^{(2)}$. However, the main focus is on the J_1 - J_2 and J_1 - J_3 models. In these models $J^{(1)}=J_1$, and $J^{(2)}$ is either the second-neighbor exchange constant J_2 , or the third-neighbor exchange constant J_3 .

As in I, the following assumptions are made: 1) Thermal equilibrium, at temperature T and magnetic field B , prevails. 2) All the magnetic ions are identical. 3) The cation sites form a square lattice, and the magnetic ions are randomly distributed over these sites. 4) Only a fraction x of all cations sites are occupied by magnetic ions. This fraction is well below the site percolation concentration x_c for the relevant cluster model. 5) None of the magnetic interactions is anisotropic. Background mate-

rial for the present paper may be found in I, in a recent review,² and in earlier papers.^{3,4,5}

This paper is organized as follows. The principal results are presented in the main text. Supplementary material is relegated to appendices. The main text starts with a brief discussion of the crucial role of cluster "configurations" in the theory. All cluster types in the J_1 - J_2 and J_1 - J_3 models, subject to the restriction $n_c \leq 5$ on the cluster size n_c , are then identified. The statistics for these cluster types is expressed using perimeter polynomials (PP's) for cluster types. As discussed in I, the PP's for cluster types are analogous to the conventional PP's for cluster sizes.⁶

The contribution of any cluster type to the magnetization M is calculated by combining the results for the energy eigenvalues with those for the cluster statistics of that cluster type. The total magnetization $M(T, B)$ is the sum of the contributions from all cluster types. In some respects the derivative curve, dM/dB versus B , is more informative than the magnetization curve, M versus B . Examples of calculated magnetization and derivative curves at constant T are given for widely different ratios $J^{(2)}/J^{(1)}$.

The statistics for cluster types is independent of the spin S of the individual magnetic ions. However, the energy eigenvalues, and therefore the magnetization curve, depend on S . Although much of the discussion is for any

S , all the numerical examples are for $S=5/2$, which is the appropriate value for the Mn^{2+} and Fe^{3+} ions. Both these ions are S -state ions, and they usually have low crystalline anisotropy. Such ions are useful for testing theories in which anisotropy is neglected.

The structures of the magnetization and derivative curves are much simpler when the ratio $J^{(2)}/J^{(1)}$ is “very small.” Cluster models with such widely different magnitudes of $J^{(2)}$ and $J^{(1)}$ are called “lopsided cluster models.” In addition to their interesting physics, lopsided models are useful because they apply to many materials. Lopsided cluster models are discussed in detail in the following paper.⁷

II. CLUSTER CONFIGURATIONS

A. Configurations

The calculation of the magnetization $M(T, B)$ in any cluster model requires: 1) the identification of all cluster types c in that model; 2) a calculation of the average magnetic moment $\mu_c(T, B)$ per realization,⁸ for each cluster type c ; and 3) an evaluation of the probabilities of finding the various cluster types.

Before carrying out the first and third of these tasks it is necessary to identify all the “cluster configurations” that exist in the particular cluster model. These cluster configurations are the fundamental building blocks of the theory, and also of the computer programs that are used to implement the theory. Cluster configurations were discussed in Sec. IIIB of I. The discussion below brings out some new features.

1. Cluster configurations

A spin cluster consists of a finite number of exchange-coupled magnetic ions (spins) that occupy a set of cation sites. Spin clusters are considered to have the same configuration if and only if the sets of cation sites occupied by these clusters can be obtained from each other by symmetry operations of the space group of the cation structure. Each one such set of cation sites is called a “realization” of the configuration.

The symmetry operations of the space group of the cation structure are the only symmetry operations considered in the present work. They will be referred to, simply, as “symmetry operations.” The symmetry operations that are relevant to the present work are the operations of the $P4m$ space group of the square lattice, including the lattice translations.

Realizations of the same configuration have the following important geometrical property. Starting from one realization, a rigid object can be constructed by joining all pairs of cation sites in that realization by straight-line segments. The straight-line segments may be viewed as “struts” that give the object its rigidity. Rigid objects

constructed in this manner from different realizations of the same configuration, either have identical shapes or are chiral isomers (mirror images) of each other. Because of this geometrical property, configurations of clusters are sometimes viewed as the geometrical shapes of clusters.

2. Cluster configurations of one specific cluster model

A cluster model is specified by the set of exchange constants (the J 's) that are included in the model. Any spin cluster in this model consists of spins that are coupled to each other, but not to other spins, by the J 's of the model. Thus, any two spins in a cluster are connected by at least one continuous path of exchange bonds associated with this set of J 's. No continuous path of such exchange bonds is allowed to exist between spins in different clusters.

The restriction on the allowed J 's is a restriction on the allowed sets of cation sites associated with the clusters of the model. For example, in the J_1 - J_2 model, any cation site of a cluster must have a NN site or a 2nd-neighbor site in the same cluster. The cluster configurations of the model are all the configurations of the sets of cation sites that are allowed by the J 's of the model.

3. Identical configurations in different cluster models

Sometimes, several cluster models are considered. It may then happen that the set of J 's in one cluster model is only a subset of all the exchange constants in another cluster model. Any cluster configuration in the cluster model with the fewer J 's is then also a configuration in the model with the larger set of J 's. For example, the exchange constant J_1 of the NN cluster model is a subset of the exchange constants in the J_1 - J_2 model. Any cluster configuration in the J_1 model is also a configuration in the J_1 - J_2 model. The converse is not true; many cluster configurations that exist in the J_1 - J_2 model do not exist in the J_1 model.

For the same reason, all cluster configurations that exist in the J_1 model also exist in the J_1 - J_3 model. Figure 2 of I shows an example of the same configuration in different cluster models. Figure 2(b) of I shows the configuration in the J_1 model, and Figs. 2(c) and 2(d) show the same configuration in the J_1 - J_2 and J_1 - J_3 models, respectively.

B. From cluster configurations to cluster types

Once a cluster model is specified, it is necessary to identify the cluster types that exist in the model. In the present work this identification was carried out by a series of computer program. The first set of programs identified all the (different) configurations that exist in

the specified cluster model. For each configuration, a realization that has one spin at the origin was generated. This realization is called the “prototype” of the configuration. Only configurations with no more than 5 cation sites were considered explicitly in the present work.

A cluster type c is specified by a cluster size n_c and by a bond list.¹ To identify the cluster types that exist in the model, the prototypes of all the (different) configurations were first classified by size, i.e., by the number of spins in the prototype. The next step was to generate the bond lists for all prototypes of a given size, n_c . The final step was to identify all prototypes of the same size n_c that have identical bond lists. Such prototypes are, by definition,⁸ realizations of the same cluster type, c . In fact, they are the prototypes of all the configurations r_c of cluster type c .

To summarize, the classification of the prototypes of different configurations by both size and bond list leads to: 1) all cluster types c , for each cluster size n_c ; 2) the bond list for each of these cluster types; and 3) the prototypes of all the configurations of each cluster type.

C. Statistics of cluster types

The goal of the statistics is to find, for each cluster type c , the probability P_c that a randomly-chosen spin is in one of the realizations of this cluster type. The main assumption is that the magnetic ions are randomly distributed over the cation sites. The procedure for calculating P_c as a function of x was outlined in Sec. III C of I. The procedure starts from the configurations r_c of cluster type c .

Any realization of cluster type c must also be a realization of one of the configurations r_c of that cluster type. The probability P_{r_c} that a randomly-chosen spin is in some realization of the configuration r_c is given by Eq. (4) of I. This equation contains two parameters that depend on the configuration: the lattice-combinatorial parameter n_{r_c} , and the perimeter ν_{r_c} . After these two parameters are evaluated for each of the configurations r_c , the probability P_c is obtained by summing P_{r_c} over all the configurations r_c of cluster type c . This sum is given by Eq. (5) of I.

The lattice-combinatorial parameter n_{r_c} is the number of (distinct) realizations of the configuration r_c that have one spin at the origin. This n_{r_c} depends only on the configuration. If the same configuration exists in more than one cluster model, then the corresponding lattice-combinatorial parameters are the same in all these models. The computer program that was used to obtain n_{r_c} was based on the principle that all realizations of a configuration can be generated from the prototype of the configuration by applying the symmetry operations of the $P4m$ space group, including the lattice translations. If the same realization was generated by different symmetry operations, the count for n_{r_c} included this realization only once.

In contrast to n_{r_c} , the perimeter ν_{r_c} depends not only on the configuration but also on the cluster model. If the same configuration exists in two cluster models, the perimeters in the two models are, in general, not equal. For example, any configuration that is present in the J_1 model is also present in the J_1 - J_2 model. The perimeter in the J_1 model will be called the J_1 perimeter. Given any realization of the configuration r_c , the J_1 perimeter is the number of (cation) sites that are NN’s of the sites in the realization, but are not themselves sites of the realization. The perimeter in the J_1 - J_2 model (called the J_1 - J_2 perimeter) is the number of sites that are either NN’s and/or 2nd-neighbors of the sites in the realization, but are not themselves sites of the realization. Therefore, for the same configuration, the J_1 - J_2 perimeter is larger than the J_1 perimeter. As a consequence, the probability that a randomly-chosen spin is in a realization of this configuration will be lower in the J_1 - J_2 model than in the J_1 model [See Eq. (4) of I]. Similar results apply to a configuration that exists in both the J_1 and the J_1 - J_3 models.

III. CLUSTER TYPES

A. Generic and specific models

A $J^{(1)}$ - $J^{(2)}$ cluster model in which the symmetry classes of the neighbors associated with $J^{(1)}$ and $J^{(2)}$ are not specified will be called a “generic” model. If the symmetry classes of the neighbors are specified, the cluster model is “specific” rather than generic. In this paper, only two specific $J^{(1)}$ - $J^{(2)}$ models are considered: the J_1 - J_2 model (with $|J_1| > |J_2|$), and the J_1 - J_3 model (with $|J_1| > |J_3|$). The reason for focusing on these specific models is that exchange constants often tend to decrease as the distance r of the relevant neighbor increases. Although the decrease is not always monotonic,^{4,5} we expect that in the vast majority of diluted antiferromagnets with a square cation lattice, $J^{(1)} = J_1$ and $J^{(2)}$ is either J_2 or J_3 .

The cluster types in the J_1 - J_2 model are not trivially related to the cluster types in the J_1 - J_3 model. That is, the bond lists for the two models cannot be obtained from each other by replacing the J_2 bonds by J_3 bonds. The site percolation concentrations for these two specific models are also different.⁹ The non-trivial dependence of the bond lists, and hence of the cluster types, on the specific cluster model implies that bond lists and cluster types cannot be given for a generic model. They can only be given for a specific model.

B. Parent cluster models

The “parent” cluster models of the J_1 - J_2 model are the J_1 model and the J_2 model, each of which has only one of exchange constants of the J_1 - J_2 model. The J_1 - J_2

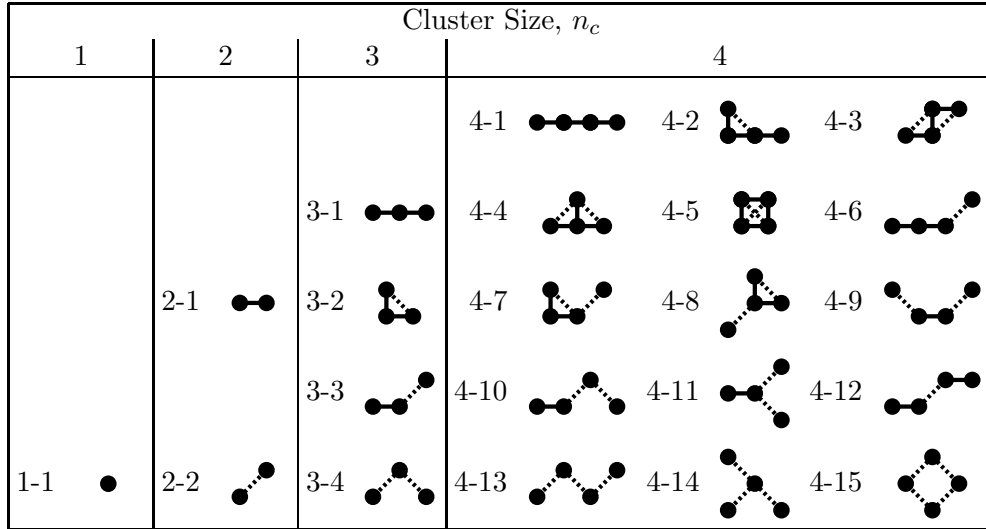


FIG. 1: Cluster types of the J_1 - J_2 model, up to cluster size $n_c=4$. Solid circles represent spins. Solid and dotted lines represent J_1 bonds and J_2 bonds, respectively. The labels for the cluster types are discussed in the text.

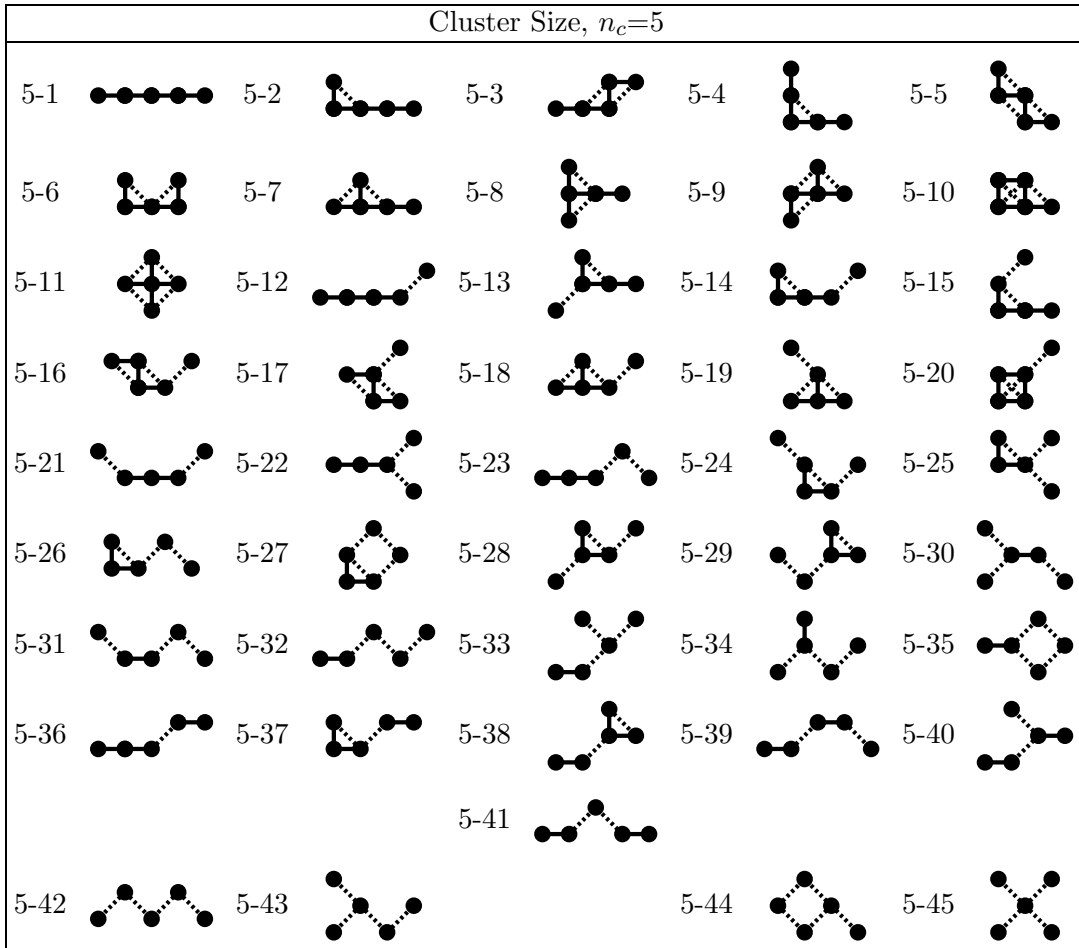


FIG. 2: Cluster types of quintets ($n_c=5$) in the J_1 - J_2 model.

model is not a simple combination of its parent models. Similarly, the J_1 - J_3 model is not a simple combination of the J_1 and J_3 models, which are its parent models.

There are many interesting relations between the J_1 - J_2 and J_1 - J_3 models and their respective parent models. To avoid repeated interruptions in the main text of the paper, discussions of these relations are relegated to Appendices. For the limited purpose of calculating magnetization curves numerically, the results in these Appendices are not essential. However, these results give a deeper insight into the physics. Some of these results will be quoted, and used, in the main texts of the present paper and of the following paper. Appendix A, describes the strong similarity (called “isomorphism”) between the three parent models, i.e., the J_1 , J_2 , and J_3 models. These are the only “parent models” considered in the present work.

C. Cluster types in the J_1 - J_2 model

1. Cluster types

In the J_1 - J_2 model on the square lattice, there are 67 cluster types of sizes $n_c \leq 5$. These cluster types are shown in Figs. 1 and 2. Cluster types of the same size, n_c , appear in the same column. The four columns in Fig. 1 show the cluster types with $n_c=1, 2, 3$, and 4. The single column in Fig. 2 shows the cluster types with $n_c=5$. Spins are represented by solid circles, J_1 bonds by solid lines, and J_2 bonds by dotted lines. Only one configuration for each cluster type is shown. The bond lists for these cluster types, which specify all intra-cluster exchange interactions,¹ are given in Appendix B.

Each cluster type is labeled by two numbers separated by a hyphen. The first number is the cluster size n_c . The second is a serial number (SN) within this cluster size. Thus, the format for any label is $[n_c\text{-(SN)}]$. There is only one type of single (type 1-1), but two types of pairs: 2-1 which is a J_1 -pair, and 2-2 which is a J_2 -pair. There are four types of triplets ($n_c=3$), 15 types of quartets ($n_c=4$), and 45 types of quintets ($n_c=5$).

2. Four categories of cluster types

The number of cluster types in Figs. 1 and 2 is rather large. It is therefore useful to classify them. The classification scheme is not unique. In one scheme the 67 cluster types in Figs. 1 and 2 are divided into four broad categories:

1. “single,” which has no exchange bonds;
2. “pure J_1 ” cluster types, with only J_1 exchange bonds;
3. “pure J_2 ” cluster types, with only J_2 bonds;
4. “mixed” cluster types, with both J_1 and J_2 bonds.

The single (type 1-1) is at the left of the bottom row of Fig. 1. The only pure J_2 cluster types are the other 5 cluster types in the same bottom row together with the four cluster types in the bottom row of Fig. 2. The only pure J_1 cluster types are: 2-1, 3-1, 4-1, and 5-1. All the remaining 53 cluster types are “mixed” types.

The pure J_1 cluster types, and the pure J_2 cluster types, are related to cluster types in the (parent) J_1 and J_2 models, respectively. These relations are discussed in Appendix C.

D. Cluster types in the J_1 - J_3 model

In the J_1 - J_3 model there are 82 cluster types of sizes $n_c \leq 5$. They are shown in Figs. 3 and 4. The format is the same as in Figs. 1 and 2, except that the dotted lines now represent J_3 bonds. The bond lists for the cluster types in Figs. 3 and 4 are given in Appendix B.

The labels for the cluster types of the J_1 - J_3 model have the same format as those for the cluster types in the J_1 - J_2 model. Therefore, many of the labels used in the two models are identical. When the same label appears in both models, it often refers to different cluster types (i.e., different bond lists). Unless it is clear from the context, it is then necessary to specify the cluster model to which the label refers.

Once again the cluster types in Figs. 3 and 4 can be divided into four categories:

1. the “single” (type 1-1), at the left of the bottom row of Fig. 3;
2. the 9 “pure J_3 ” cluster types, consisting of the other 5 cluster types in the bottom row of Fig. 3 together with the 4 cluster types in the bottom row of Fig. 4;
3. the 5 “pure J_1 ” cluster types: 2-1, 3-2, 4-3, 4-5, and 5-5;
4. the 67 remaining cluster types, which are all “mixed” types.

IV. CLUSTER STATISTICS AND PERIMETER POLYNOMIALS

A. Results for small clusters

The probabilities P_c as a function of x were obtained using the procedure discussed in Sec. II C. Only cluster types with $n_c \leq 5$ were considered. Some of the results for the J_1 - J_2 model are shown Fig. 5. They include the P_c 's for the single (type 1-1), for the two types of pairs (2-1 and 2-2), and for the four types of triplets (3-1, 3-2, 3-3 and 3-4). These labels for the cluster types refer to Fig. 1. Also shown in Fig. 5 are: the sum P_4 of the probabilities for all 15 quartet types in Fig. 1; the sum P_5 of the probabilities for all the quintet types in Fig. 2;

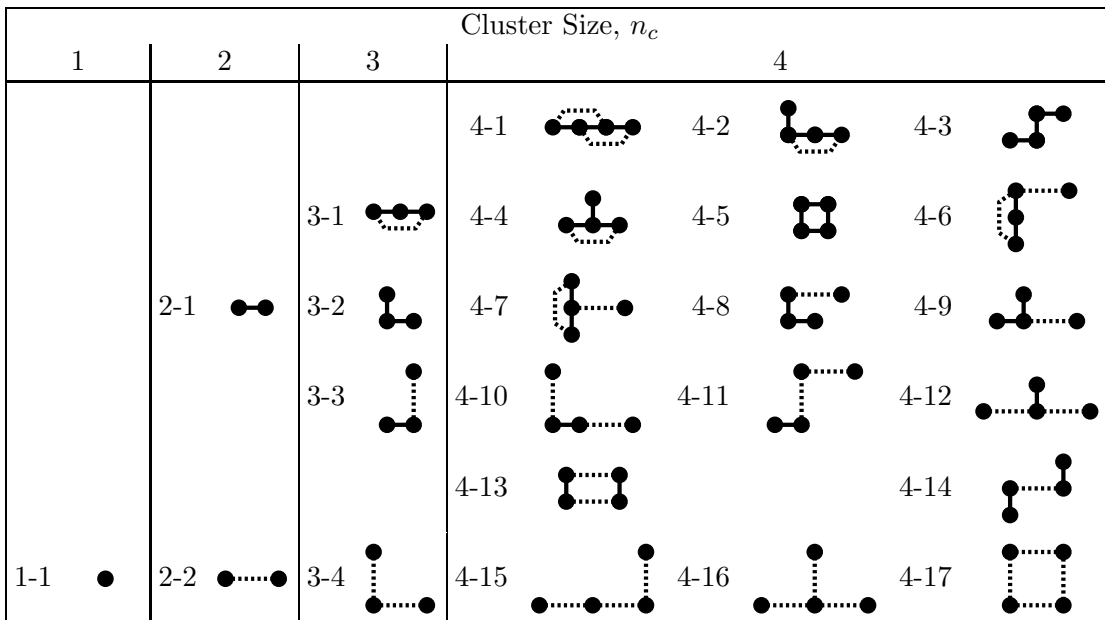


FIG. 3: Cluster types of the J_1 - J_3 model, up to cluster size $n_c=4$. The format, including the format of the labels for the cluster types, is similar to that in Fig. 1, except that the dotted lines represent J_3 bonds.

and the sum $P_{>5}$ of the probabilities for all cluster types with sizes $n_c > 5$.

Figure 6 shows the corresponding probabilities for the J_1 - J_3 model. In this case the cluster types refer to Figs. 3 and 4. In both Fig. 5 and Fig. 6 the highest value of x is below the relevant site percolation concentration, $x_c=0.407$ for the J_1 - J_2 model, and $x_c=0.337$ for the J_1 - J_3 model.^{9,10} For the J_1 model, $x_c=0.593$.

B. Perimeter polynomials

As discussed in I, the probability P_c can be expressed succinctly in the form

$$P_c = n_c x^{n_c-1} D_c(q), \quad (1)$$

where $D_c(q)$ is a polynomial in $q=1-x$, defined as the perimeter polynomial (PP) for cluster type c . Appendix B gives the PP's for cluster types with sizes $n_c \leq 5$ in the J_1 - J_2 model. These are the cluster types in Figs. 1 and 2. Appendix B also gives the PP's for cluster types of the J_1 - J_3 model whose sizes are $n_c \leq 5$. These are the cluster types in Figs. 3 and 4.

For the J_1 - J_2 model, the following check on the results for $D_c(q)$ in Appendix B was performed. The conventional PP's, $D(q)$, for cluster sizes (not types) were given for this model by Peters et al.¹⁰ As expected, the polynomial $D(q)$ for any cluster size s is equal to the sum $\sum D_c(q)$ of the PP's in Appendix B over all cluster types c that have the size $n_c=s$.

Appendix D discusses some relations between the probabilities P_c for the pure- J_1 and pure- J_2 cluster types in

the J_1 - J_2 model and the probabilities for the same cluster types in the (parent) J_1 and J_2 models. The relations between the probabilities P_c for pure- J_1 and pure- J_3 cluster types in the J_1 - J_3 model and the probabilities for the same cluster types in the (parent) J_1 and J_3 models are also discussed.

V. THE MAGNETIZATION CURVE

A. Calculation procedure

The procedure for calculating the magnetization $M(T, B)$ was discussed previously.^{1,2} Briefly, the Hamiltonian of one realization⁸ of each cluster type c is diagonalized, and the results are used to obtain the average magnetic moment $\mu_c(T, B)$ per realization. For singles, $\mu_c(T, B)$ follows the Brillouin function for spin S . For each of the other cluster types, $\mu_c(T, B)$ exhibits a series of MST's as a function of B at very low T .

The total magnetization $M(T, B)$ is a statistically-weighted sum of $\mu_c(T, B)$. This sum is given by Eq. (13) of I, namely,

$$M(T, B) = \sum_c N_c \mu_c(T, B) = N_{\text{total}} \sum_c \frac{P_c}{n_c} \mu_c(T, B), \quad (2)$$

where $N_c = P_c N_{\text{total}} / n_c$ is the population of cluster type c , and N_{total} is the total number of spins. The quantities M , N_c and N_{total} are all either per unit mass or per unit volume.

The infinite sum in Eq. (2) cannot be evaluated exactly because $\mu_c(T, B)$ and P_c (or N_c) are known only for a fi-

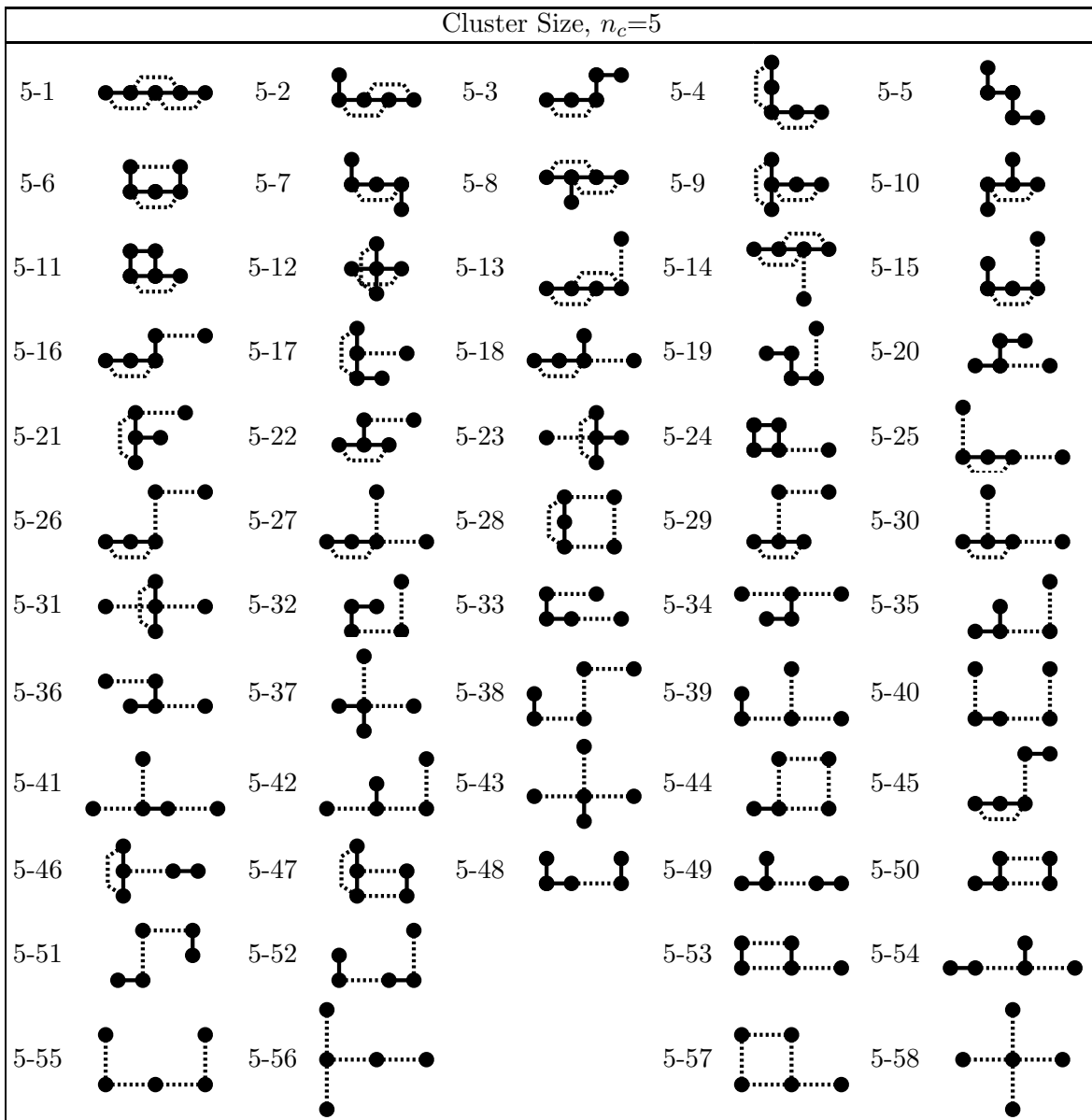


FIG. 4: Cluster types of quintets ($n_c=5$) in the J_1 - J_3 model.

nite number of cluster types c . Usually they are known only for cluster types whose sizes n_c are no larger than some maximum size n_{\max} . The sum in Eq.(2) is therefore truncated after the finite sum over cluster types with $n_c \leq n_{\max}$ is evaluated exactly. The remainder (REM) from clusters of sizes $n_c > n_{\max}$, is then approximated by the “remainder correction” $R(T, B)$. In the present work, $n_{\max}=5$, so that the REM is from clusters larger than quintets. The remainder correction $R(T, B)$ was obtained by the corrective quintets (CQUIN’s) method. The application of this method to the NN cluster model was discussed in I. For a model with two exchange constants the CQUIN’s method is considerably more involved.

The number of spins in the REM is $P_{>5}N_{\text{total}}$. The accuracy of the CQUIN’s method is not an important issue

if $P_{>5} \ll 1$. Because $P_{>5}$ increases with x , the accuracy is not a significant issue if x is sufficiently small. All magnetization curves in the present paper are for $x \leq 0.09$, and are based on the J_1 - J_2 model. Under these conditions, $P_{>5} \leq 3.6\%$, so that errors in M resulting from the CQUIN’s method are not significant. The description of the CQUIN’s method is postponed to the following paper, which also includes some examples for higher x .

B. The two reduced magnetic fields

The two exchange constants, $J^{(1)}$ and $J^{(2)}$, lead to two energy scales for the Zeeman energy. In analogy to Eq. (10) of I, the primary reduced magnetic field b_1 is

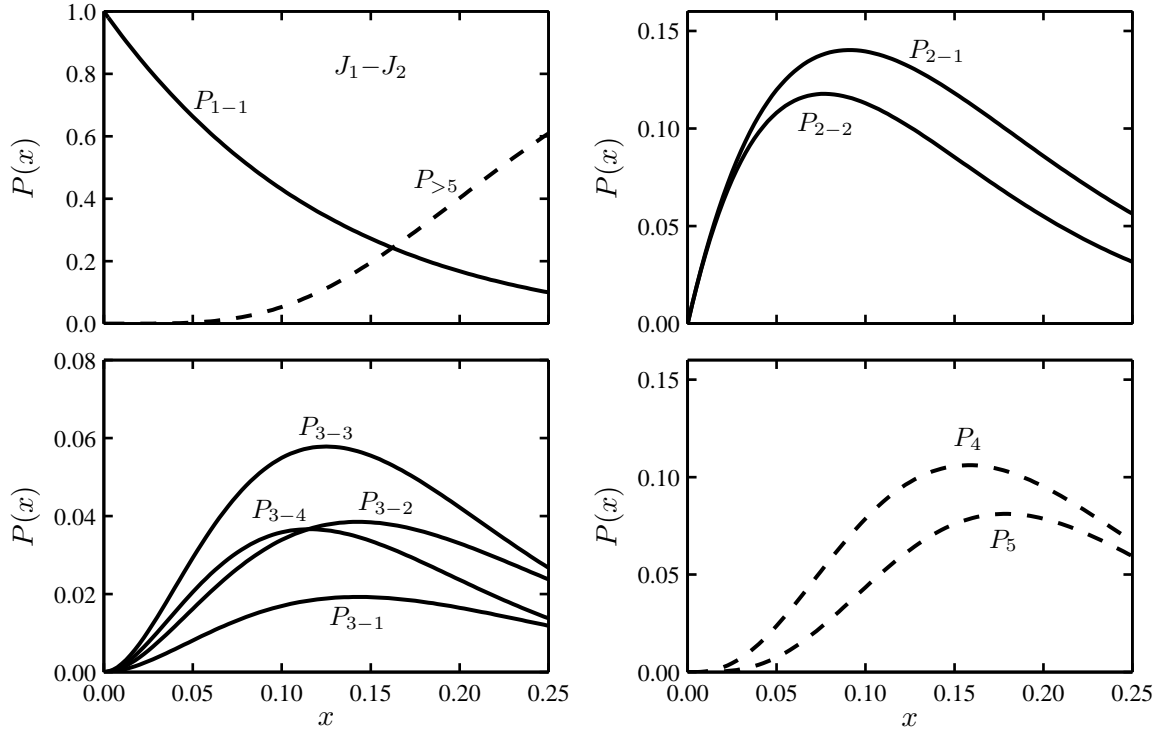


FIG. 5: Probabilities P_c as a function of x for some cluster types of the J_1 - J_2 model. The solid curves are for individual cluster types, labeled as in Fig. 1. Curve 1-1 is for singles, curves 2-1 and 2-2 are for the two types of pairs, and curves 3-1 up to 3-4 are for the four types of triplets. The dashed curves are probabilities for some combinations of cluster types: P_4 is the sum of the P_c 's for all the 15 quartet types in Fig. 1; P_5 is the sum of the P_c 's for all 45 quintet types in Fig. 2; and $P_{>5}$ is the sum of the probabilities for all cluster types of sizes $n_c > 5$.

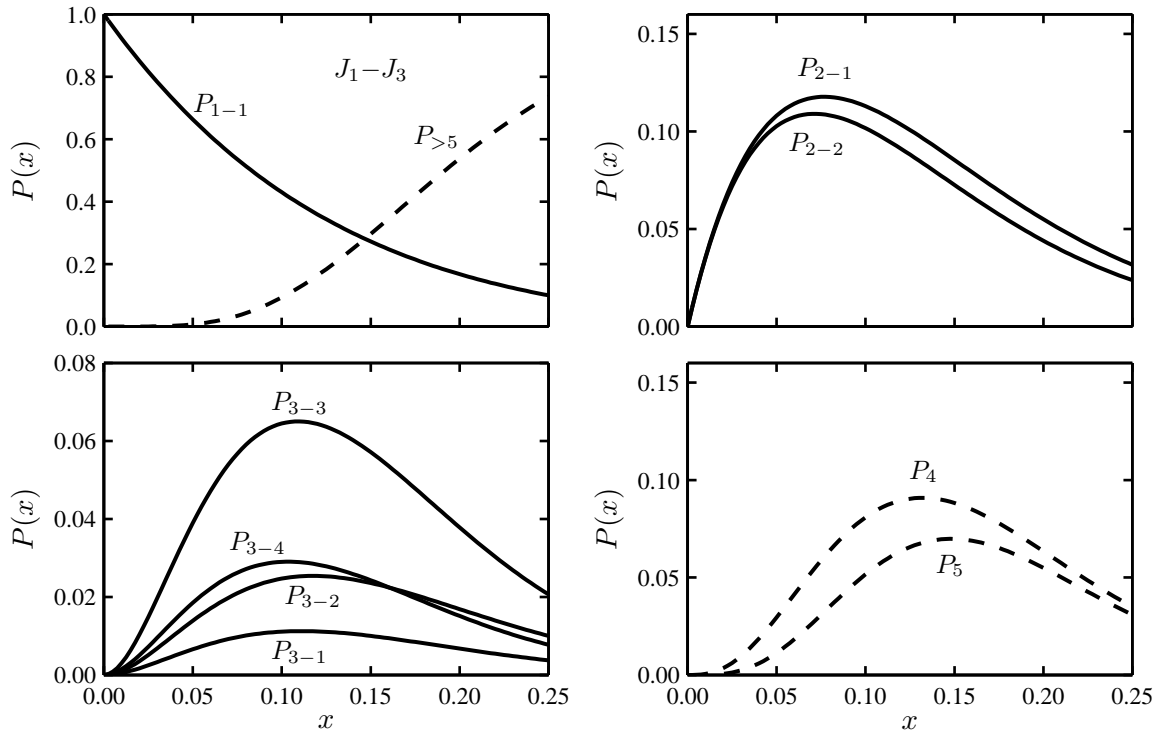


FIG. 6: Probabilities P_c as a function of x for some cluster types of the J_1 - J_3 model. The labels for the various curves are similar to those in Fig. 5, except that the cluster types refer to Figs. 3 and 4 for the J_1 - J_3 model.

defined as

$$b_1 = g\mu_B B / |J^{(1)}|. \quad (3a)$$

The secondary reduced magnetic field b_2 is

$$b_2 = g\mu_B B / |J^{(2)}|. \quad (3b)$$

Thus, at any given B ,

$$b_1/b_2 = |J^{(2)}/J^{(1)}| < 1. \quad (4)$$

The reduced magnetization m is defined as in I. That is,

$$m = M/M_0, \quad (5)$$

where M_0 is the true saturation value of M . The reduced parameters b_1 , b_2 , and m , will be used in plots and discussions of the magnetization curves.

C. MST's from the two different types of pairs

At a low T the calculated magnetization curve, M versus B , includes a superposition of many series of MST's. Each series arises from some cluster type c of size $2 \leq n_c \leq n_{\max}$. The magnitude $(\Delta M)_c$ of a magnetization jump at each MST in the series is proportional to the population N_c of the relevant cluster type. For low x the largest jumps $(\Delta M)_c$ are for $J^{(1)}$ pairs and $J^{(2)}$ pairs. In both J_1 - J_2 and J_1 - J_3 models these pairs are cluster types 2-1 and 2-2, respectively (see Figs. 1 and 3).

The MST's from $J^{(1)}$ pairs occur at the primary reduced fields

$$b_1 = 2, 4, 6, \dots, 4S. \quad (6a)$$

The MST's from $J^{(2)}$ pairs occur when the secondary reduced field has the same values, i.e., at

$$b_2 = 2, 4, 6, \dots, 4S. \quad (6b)$$

Experimental values of the magnetic fields B at the MST's from pairs are often used to determine $J^{(1)}$ and $J^{(2)}$. The temperature requirement for resolving the MST's from $J^{(2)}$ pairs is $k_B T < |J^{(2)}|$. This is a more stringent requirement than $k_B T < |J^{(1)}|$ for resolving the MST's from $J^{(1)}$ pairs.

Equations (6a) and (6b) use the reduced fields b_1 and b_2 . Using the magnetic field B , instead of the reduced fields, the ranges of B for the MST series from the two types of pairs may or may not overlap. The condition for avoiding overlap is

$$J^{(2)}/J^{(1)} < 1/2S. \quad (7)$$

For magnetic ions with $S=5/2$ (e.g., Mn^{2+} or Fe^{3+}) overlap is avoided if $J^{(2)}/J^{(1)} < 0.2$.

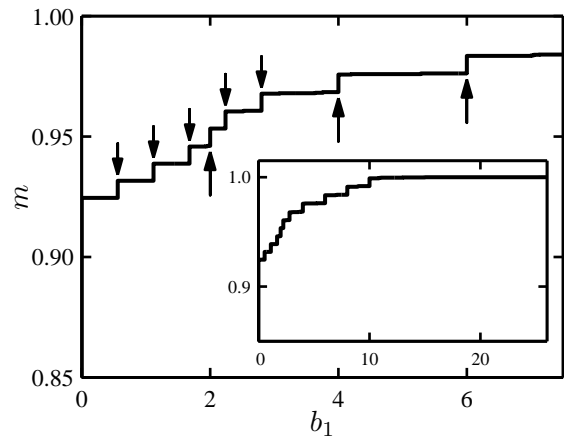


FIG. 7: Magnetization curve at $T=0$, calculated from the J_1 - J_2 model using the parameters $x=0.01$, $S=5/2$, and $J_2/J_1=0.28$. The ordinate is the reduced magnetization, $m=M/M_0$, where M_0 is the true saturation magnetization. The abscissa is the primary reduced magnetic field $b_1=g\mu_B B/|J_1|$, up to 7.5. MST's from J_1 pairs (cluster type 2-1) are indicated by long upward arrows. MST's from J_2 pairs (cluster type 2-2) are indicated by shorter downward arrows. The inset shows the full magnetization curve, up to complete saturation.

D. Two examples of magnetization curves for very low x

The main purpose of the following two examples is to illustrate the dependence of the MST pattern on the ratio $J^{(2)}/J^{(1)}$. The examples are for $x=0.01$ in the J_1 - J_2 cluster model. To optimize the resolution of the spectra, the examples are for $T=0$. The value $S=5/2$ is assumed.

Figures 7 and 8 are for $J_2/J_1=0.28$. Figure 7 shows the reduced magnetization m as a function of the primary reduced magnetic field b_1 . MST's from J_1 pairs (cluster type 2-1) are indicated by long arrows, and those from J_2 pairs (cluster type 2-2) by shorter arrows. The main part of Fig. 7 shows the magnetization curve up to $b_1 = 7.5$. The full magnetization curve is shown in the inset.

Figure 8 shows the derivative dM/dB , in normalized units,¹¹ in fields up to $b_1 = 7$, corresponding to the main part of Fig. 7. The upper abscissa scale is for the secondary reduced magnetic field b_2 . The derivative peaks at MST's from J_1 -pairs (type 2-1) and from J_2 -pairs (type 2-2), are indicated by long and short arrows, respectively. Their reduced magnetic fields are given by Eqs. (6a) and (6b). Because the ratio $J_2/J_1=0.28$ is higher than 0.2, the field ranges for the series of MST's from the two types of pairs overlap.

Figure 9 shows the magnetization (top) and derivative (bottom) curves for $x=0.01$ when the ratio $J_2/J_1=0.028$, i.e., smaller by a factor of 10 compared to the ratio in Figs. 7 and 8. All other parameters are the same as for Figs. 7 and 8. Because the ratio J_2/J_1 is now well below 0.2, the MST series from J_1 - and J_2 -pairs occur in field ranges that do not overlap. In the "gap" between

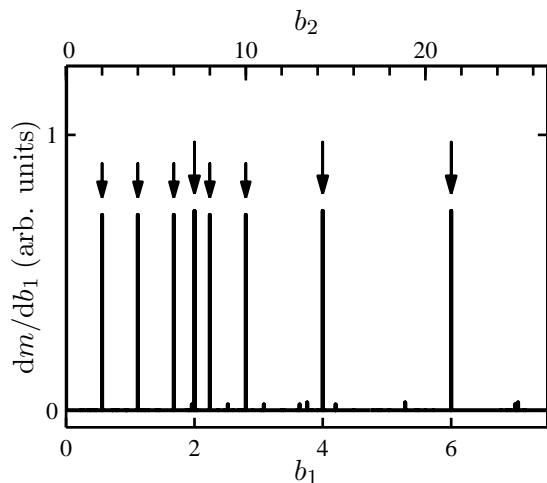


FIG. 8: The derivative of the magnetization curve in Fig. 7. The ordinate is the derivative $dm/db_1 = (|J_1|/g\mu_B M_0)(dM/dB)$. The lower abscissa scale is for the primary reduced field b_1 . The upper abscissa scale is for the secondary reduced magnetic field b_2 . The derivative peaks at MST's from cluster types 2-1 (J_1 pairs) and 2-2 (J_2 pairs) are indicated by long and short arrows, respectively.

these two field ranges, the magnetization (upper curve) exhibits a plateau of apparent saturation, labeled as m_s . The apparent saturation value, $m_s=0.961$, agrees with the value of m_s obtained from the NN cluster model for this x (Ref.1). However, in contrast to the NN cluster model, the apparent saturation is reached only after the series of MST's from the J_2 pairs (type 2-2) is completed. Clearly, the MST pattern for $J_2/J_1=0.028$ (Fig. 9) is much simpler than that for $J_2/J_1=0.28$ (Figs. 7 and 8).

Figure 7 for $J_2/J_1=0.28$ shows a short magnetization plateau immediately after the initial magnetization rise. This plateau, which ends at the first MST from J_2 pairs (not J_1 pairs), is not the plateau of apparent saturation predicted by the NN cluster model. The value $m=0.925$ at the first short plateau in Fig. 7 is well below the apparent saturation value $m_s=0.961$ in the NN cluster model. The reason for the lower value is that the series of MST's from J_2 pairs has not been completed before the start of this short plateau.

VI. THE MST SPECTRUM

A. Spectrum

The derivative dM/dB as a function of B exhibits a peak at each MST. The pattern of the peaks in the derivative curve will be called the ‘‘MST spectrum.’’ Figure 8 and the lower curve in Fig. 9 are examples of such MST spectra. Each peak in dM/dB is a ‘‘spectral line.’’ Two or more spectral lines associated with MST's arising from different cluster types may overlap. When a spectral line

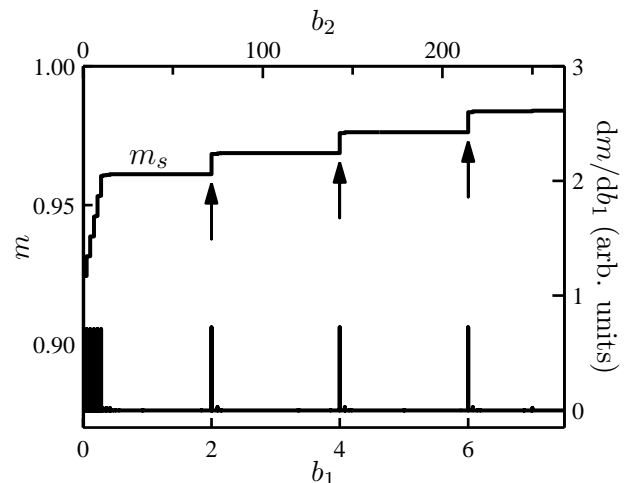


FIG. 9: Zero-temperature magnetization curve (upper curve) and its derivative (lower curve) for $x=0.01$. These curves are calculated using the J_1 - J_2 model and the ratio $J_2/J_1=0.028$. As in Fig. 8 the lower and upper abscissa scales are for b_1 and b_2 , respectively. The left ordinate scale is for m . The right ordinate scale is for dm/db_1 . The arrows indicate the locations of the MST's from J_1 pairs (type 2-1). The MST's from J_2 pairs (type 2-2) are bunched up at low fields. The plateau of apparent saturation is labeled as m_s .

is due to only one MST from one cluster type c , the integral of the spectral line with respect to B is equal to the magnetization jump $(\Delta M)_c$.

There are several advantages of using the spectrum. A plot of the spectrum, dM/dB versus B , is very effective in conveying information visually. Another advantage is that the calculated spectrum is the *exact* spectrum from cluster types with $n_c \leq n_{\max}$.

As discussed earlier, the infinite sum in Eq. (2) is split into a sum over clusters with $n_c \leq n_{\max}$, and a remainder (REM) from larger clusters ($n_c > 5$ in the present work). The reason for the split is that the Hamiltonians of clusters with $n_c > n_{\max}$ have not been diagonalized. The finite sum is evaluated exactly, but the REM is approximated by $R(T, B)$. The derivative of $R(T, B)$ does not give the spectral lines from the clusters with $n_c > n_{\max}$. These lines can be obtained only if cluster Hamiltonians for $n_c > n_{\max}$ are diagonalized.

A wealth of information, such as accurate exchange constants, can be obtained from a comparison of an experimental spectrum with the calculated exact spectrum for $n_c \leq n_{\max}$. All the spectra shown in this paper are the derivatives of the exact finite sum up to $n_{\max}=5$, without the remainder (see Ref. 12).

B. Additional examples of MST patterns and spectra

The examples in Sec. VD, for $J_2/J_1=0.28$ and 0.028 , assumed $x=0.01$. The following examples are for the

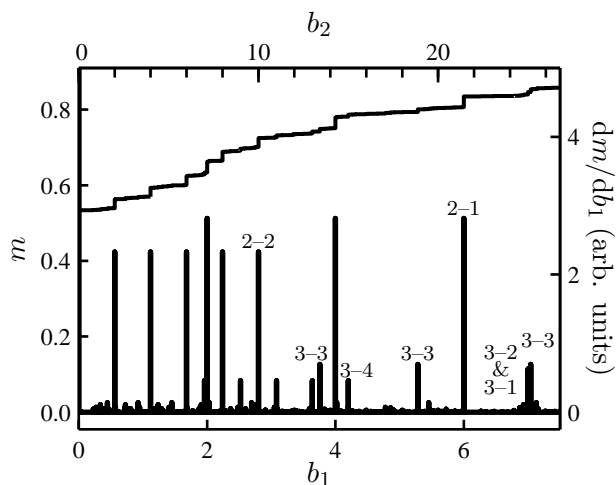


FIG. 10: The reduced magnetization m (top curve) and the MST spectrum (lower curve) at $T=0$ for $x=0.09$, $S=5/2$. These curves are for $J_2/J_1=0.28$. Only the results in the range $b_1 < 7.5$ are shown. The cluster types responsible for some of the spectral lines are indicated.

same ratios J_2/J_1 , but for higher x . All other parameters ($S=5/2$, $T=0$), and the cluster model (J_1 - J_2), are the same as in Sec. VD. An example of a zero-temperature spectrum calculated from the J_1 - J_3 model will be given in the following paper.⁷ Calculated spectra at finite temperatures will be shown in Ref. 13 in connection with analysis of experimental data.

1. Magnetization curves and spectra for $x=0.09$

Magnetization curves and spectra for $x=0.09$ are shown in Figs. 10 and 11. From Fig. 5 the probabilities P_c for all four triplet types increase when x changes from 0.01 to 0.09. The largest increase is for triplet type 3-3, which is a J_1 pair attached to a third spin by a J_2 bond. As a result, spectral lines from type 3-3 triplets are readily seen in Figs. 10 and 11.

Figure 10 shows the MST pattern (top curve) and the MST spectrum (lower curve) for $x=0.09$ when $J_2/J_1=0.28$. The range of the primary reduced field is $b_1 < 7.5$. The cluster types responsible for some prominent spectral lines are indicated. Clearly, for $J_2/J_1 = 0.28$ the spectrum is quite complicated because of the overlap between different series of MST's from different cluster types.

Figure 11 shows the results for the same x when $J_2/J_1=0.028$. For this much lower J_2/J_1 ratio, the spectrum is much simpler. All the discernable spectral lines occur in two separate field ranges. The top of the low-field range is slightly above $b_1=0.42$ where the series from type 3-4 triplets ends. The bottom of the high-field range is near $b_1=0.935$ where a small MST from quartet type 4-2 is barely discernable. The two field ranges are separated by a gap, i.e., by a field range in which there are

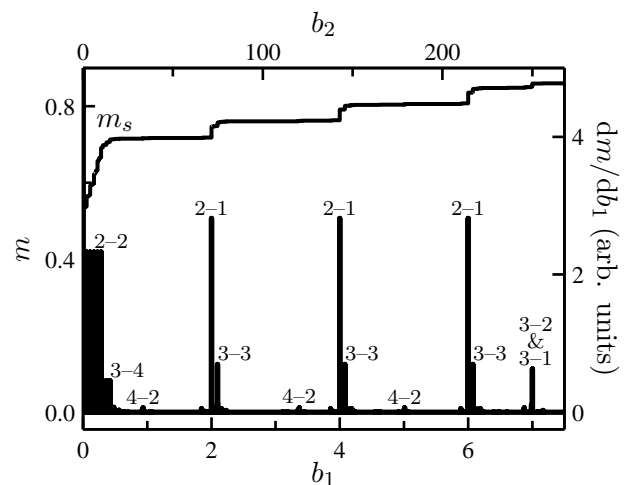


FIG. 11: Zero-temperature magnetization curve (top curve) and spectrum (lower curve) for $x=0.09$, calculated from the J_1 - J_2 model when $J_2/J_1=0.028$. The range of the primary reduced field is limited to $b_1 < 7.5$. The plateau of apparent saturation is labeled as m_s .

no discernable spectral lines. The absence of discernable lines implies that m has reached a plateau. The value $m=0.715$ at this plateau agrees with the apparent saturation value m_s calculated from the NN cluster model.

In the field range of Fig. 11 the J_1 pairs, which exist both in the J_1 and the J_1 - J_2 models, give rise to large MST's at $b_1=2, 4, 6$. These are the 2-1 lines in Fig. 11. Near each 2-1 line there is also a line from the 3-3 triplets. The 3-3 lines do not exist in the J_1 model. Each 3-3 line together with the stronger nearby 2-1 line may be viewed as a fine structure (FS) that has evolved from a single spectral line, due to J_1 pairs, in the J_1 model. The separation Δb_2 , in the secondary reduced field, between the 3-3 line and the nearby 2-1 line is of order 1. The corresponding magnetic field separation ΔB is $g\mu_B\Delta B \sim |J_2|$.

Figure 11 also shows a spectral line at $b_1=7$ labeled as 3-2 & 3-1. It corresponds to the coincidence of the first MST from triplets of type 3-1 and the first MST from triplets of type 3-2. The "intensity" of this combined line is just the sum of the two intensities. The other lines from the 3-1 and 3-2 triplets, at $b_1=9, 11, 13$ and 15 (above the field range of Fig. 11), also coincide when $J_2/J_1=0.028$. Figure 10 shows that the 3-1 and 3-2 lines still coincide when $J_2/J_1=0.28$. It can be shown that this remains true as long as $J_2/J_1 \leq 1$. For additional details see Ref. 14.

2. Spectrum for $x=0.20$

For $x=0.20$, approximately 40% of the spins are in clusters of sizes $n_c \geq 5$ (see Fig. 5). When such a large fraction of the spins are in the REM of Eq. (2), the accuracy of the CQUIN's method of treating the magnetization from the REM is open to question. Under these circumstances,

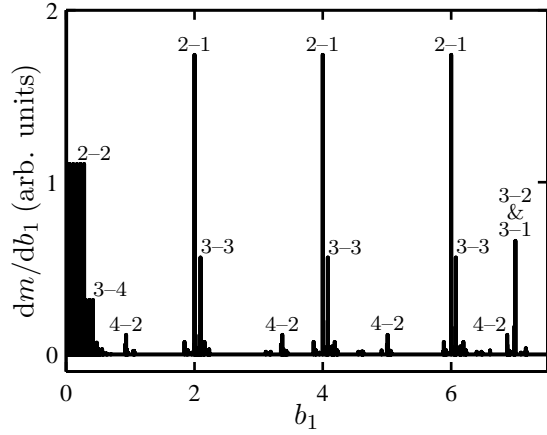


FIG. 12: Zero-temperature spectrum in the J_1 - J_2 model for $J_2/J_1=0.028$ when $x=0.20$. Cluster types responsible for some spectral lines are indicated.

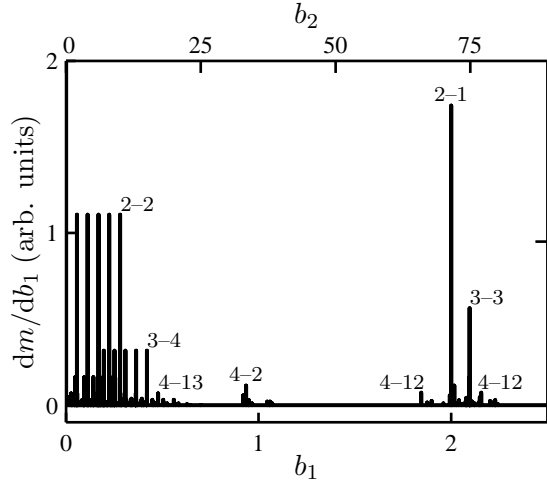


FIG. 13: Expanded view of the spectrum in Fig. 12 ($x=0.20$) for the range $0 < b_1 < 2.5$.

a plot of the exact spectrum for clusters with $n_c \leq 5$ is probably preferable to a plot of the magnetization curve.

The calculated spectrum for $x=0.20$ will be shown only for the low ratio $J_2/J_1=0.028$. Figure 12 shows this spectrum in the range $0 < b_1 < 7.5$, at $T=0$. Cluster types responsible for some of the spectral lines are indicated. An expanded view of the spectrum in the range $b_1 < 2.5$ is shown in Fig. 13. The comparison of Figs. 12 and 13 with Fig. 11 shows that the increase of x from 0.09 to 0.20 has led to the following changes:

1. There are new discernable lines. Some of these new lines are in the FS near $b_1=2$. Two of the lines in this FS are from cluster type 4-12. One of these 4-12 lines is slightly above the 2-1 line (from pure J_1 pairs in the J_1 - J_2 model), and the other 4-12 line is slightly below it. Actually there is even a stronger new line in the same FS from quartets of type 4-10. However, this line is not resolved be-

cause it is very close to the still stronger line from the 3-3 triplets.

2. A gap, in which there are no discernable spectral lines, separates the low-field and high-field parts of the spectrum. On the scale of Fig. 13 there are no discernable lines between $b_1=0.63$ and $b_1=0.92$.

VII. LOPSIDED MODELS

The spectra for a “very small” ratio J_2/J_1 , are shown in Figs. 9, and 11–13. These spectra are relatively simple. They suggest¹⁵ the following five features for such small J_2/J_1 ratios.

1. The spectrum consists of a low-field part and a high-field part, separated by a gap in which there are no discernable spectral lines.
2. In the field range of the gap, the magnetization exhibits apparent saturation, with an apparent saturation value m_s equal to that given by the NN cluster model.
3. In the high-field part of the spectrum, many spectral lines that exist in the parent J_1 model develop a FS. The most conspicuous FS evolves from those lines in the J_1 model that are due to J_1 -pairs, i.e., the lines at $b_1=2, 4, 6$, etc.
4. Separations between adjacent lines in the FS that has evolved from a single line in the J_1 model are of order $\Delta b_2 \sim 1$. The corresponding separations ΔB are of order $g\mu_B B \Delta B \sim |J_2|$.
5. In the low-field part of the spectrum, the separations between adjacent lines are also of order $\Delta b_2 \sim 1$, or $g\mu_B B \Delta B \sim |J_2|$.

The same five features are also found in simulations that use the J_1 - J_3 model when the ratio J_3/J_1 is “very small.”

When the ratio $J^{(2)}/J^{(1)}$ is sufficiently small that the five features listed above appear in the spectrum, the $J^{(2)}$ - $J^{(1)}$ model is called “lopsided.” Spectra from lopsided models are discussed in detail in the following paper. Far from a mere curiosity, lopsided models actually apply to many materials. In Ref. 13, which appears in this issue, the theoretical results for lopsided models will be used to interpret data obtained in $(C_3NH_3)_2Mn_xCd_{1-x}Cl_4$ near 20 mK.

Acknowledgments

This work was supported by CNPQ and FAPESP. Travel funds for Y. S. were also provided by FAPESP.

APPENDIX A: ISOMORPHISM OF THE PARENT J_1 , J_2 , AND J_3 MODELS

Starting from Fig. 1 of I, and using symmetry arguments¹⁶ one can show that the cluster types of the

J_1 -model, of the J_2 -model, and of the J_3 -model, are identical except for the difference in the symmetry class of the neighbor associated with the (only one) exchange constant J that is included in the model. That is, the bond lists for all cluster types in the J_2 model can be obtained from those in the J_1 model by replacing the label 1 for NN's by the label 2 for 2nd neighbors. The bond lists in the J_3 model are also the same, except that the label 3 for the 3rd neighbors replaces the label 1. Different cluster models, each with only one exchange constant, whose bond lists are related in this manner will be called "isomorphic." Corresponding cluster types in isomorphic cluster models will be called isomorphic cluster types.

The exchange part of the cluster Hamiltonian is specified by the bond list for that cluster type.¹ Cluster Hamiltonians of isomorphic cluster types are identical except for the numerical value of the only J (see Ref. 17). Each cluster type, except the single, leads to a series of MST's. The magnetic fields at the MST's originating from isomorphic cluster types are the same except for a scale factor which is proportional to the J in the model.

For the three parent cluster models considered here, the probabilities P_c for isomorphic cluster types are the same. The site percolation concentrations for these three models are also the same.⁹ It is noteworthy that for the square lattice the J_4 -model is not isomorphic to the J_1 , J_2 , and J_3 models. This difference can be understood from Fig. 1 of I. The number of 4th neighbors surrounding the central cation site is 8, compared to 4 for the 1st, 2nd, and 3rd neighbors.

APPENDIX B: BOND LISTS AND PERIMETER POLYNOMIALS FOR THE J_1 - J_2 AND THE J_1 - J_3 CLUSTER MODELS

Tables I and II in give the bond lists, and the perimeter Polynomials, $D_c(q)$, for the cluster types of the J_1 - J_2 model. The cluster types c , limited to sizes $n_c \leq 5$, are those shown in Figs. 1 and 2.

Tables III and IV in this Appendix give the bond lists, and the perimeter Polynomials, $D_c(q)$, for the cluster types of the J_1 - J_3 model. The cluster types c are those shown in Figs. 3 and 4.

APPENDIX C: RELATIONS BETWEEN "PURE" CLUSTER TYPES AND CLUSTER TYPES IN THE PARENT MODELS

Consider first the cluster types of the J_1 - J_2 model (Figs. 1 and 2). At the bottom of these figures are the "single" (type 1-1) and the nine pure J_2 cluster types. Together, they are identical to the 10 cluster types of the (parent) J_2 model. As pointed out in Appendix A the cluster types of the J_2 model are isomorphic to the cluster types of the J_1 model. The pictorial representations of the cluster types of the J_1 model, shown earlier

Cluster type, c	Bond List	$D_c(q)$
1-1	{}	q^8
2-1	{1}	$2q^{10}$
2-2	{2}	$2q^{12}$
3-1	{11;0}	$2q^{12}$
3-2	{11;2}	$4q^{12}$
3-3	{12;0}	$8q^{14}$
3-4	{22;0}	$4q^{15}+2q^{16}$
4-1	{110;01;0}	$2q^{14}$
4-2	{121;10;0}	$8q^{14}$
4-3	{112;21;0}	$4q^{14}$
4-4	{111;22;0}	$4q^{14}$
4-5	{211;11;2}	q^{12}
4-6	{110;02;0}	$8q^{16}$
4-7	{110;22;0}	$8q^{15}+8q^{16}$
4-8	{112;20;0}	$4q^{16}$
4-9	{120;02;0}	$8q^{18}$
4-10	{120;00;2}	$16q^{17}+8q^{18}$
4-11	{122;00;0}	$4q^{17}$
4-12	{210;01;0}	$8q^{16}$
4-13	{220;02;0}	$4q^{18}+8q^{19}+2q^{20}$
4-14	{222;00;0}	$4q^{18}$
4-15	{022;22;0}	q^{17}

TABLE I: Bond lists and perimeter polynomials $D_c(q)$ for cluster types of sizes $1 \leq n_c \leq 4$ in the J_1 - J_2 model. The labels for the cluster types are as in Fig. 1.

in Fig. 3 of I, are therefore also applicable to the cluster types of the J_2 model.

There are only four pure J_1 cluster types in the J_1 - J_2 model. Together with the single, they comprise only a subset of the 10 cluster types of the parent J_1 model (Fig. 3 of I). The reason why some cluster types of the J_1 model are not among the pure J_1 cluster types of the J_1 - J_2 model is the following. As discussed in Sec. II A 3, all cluster configurations that are present in the J_1 model are also present in the J_1 - J_2 model. Some of these configurations have two J_1 bonds that are: 1) connected to the same spin, and 2) make a 90° angle with each other. In the J_1 - J_2 model, each such configuration has at least one J_2 bond, so that it is a configuration of a mixed cluster of the J_1 - J_2 model, not a configuration of a pure J_1 cluster. If all configurations of a particular cluster type c of the J_1 model contain consecutive J_1 bonds that make a 90° angle, then this cluster type is not among the pure J_1 cluster types of the J_1 - J_2 model.

Two J_1 bonds that are connected to the same spin are either at a 90° angle or at a 180° angle with each other. Consider the pure J_1 cluster types that exist in the J_1 - J_2 model. Each such cluster type has only one configuration in this model. All the spins in this configuration are on a single straight line. In the parent J_1 model, on the other

Cluster type, c	Bond List	$D_c(q)$	c	Bond List	$D_c(q)$
5-1	{0110;101;00;0}	$2q^{16}$	5-23	{1100;020;00;2}	$16q^{19}+8q^{20}$
5-2	{1120;010;01;0}	$8q^{16}$	5-24	{1100;220;02;0}	$8q^{19}+4q^{20}$
5-3	{1210;120;01;0}	$8q^{16}$	5-25	{1100;222;00;0}	$8q^{18}$
5-4	{2110;101;00;0}	$4q^{16}$	5-26	{1100;220;00;2}	$8q^{18}+24q^{19}+8q^{20}$
5-5	{1122;210;01;0}	$4q^{16}$	5-27	{1100;220;02;2}	$4q^{17}$
5-6	{1122;010;01;0}	$4q^{15}+4q^{16}$	5-28	{1120;202;00;0}	$8q^{19}+8q^{20}$
5-7	{1110;201;20;0}	$8q^{16}$	5-29	{1120;200;00;2}	$8q^{19}+4q^{20}$
5-8	{1110;221;00;0}	$4q^{16}$	5-30	{1022;200;00;0}	$8q^{21}$
5-9	{1112;201;20;0}	$8q^{16}$	5-31	{1200;002;20;0}	$8q^{20}+24q^{21}+16q^{22}$
5-10	{1121;212;10;0}	$8q^{14}$	5-32	{1200;000;20;2}	$16q^{20}+32q^{21}+8q^{22}$
5-11	{1111;022;22;0}	q^{16}	5-33	{1200;000;22;0}	$24q^{20}$
5-12	{1100;010;02;0}	$8q^{18}$	5-34	{1220;000;02;0}	$8q^{20}+8q^{21}$
5-13	{1102;210;00;0}	$8q^{18}$	5-35	{1022;000;22;0}	$4q^{19}$
5-14	{1120;010;02;0}	$16q^{18}$	5-36	{1010;200;01;0}	$16q^{18}$
5-15	{1210;100;02;0}	$8q^{17}+8q^{18}$	5-37	{1100;220;00;1}	$16q^{17}+16q^{18}$
5-16	{1120;210;02;0}	$8q^{17}+8q^{18}$	5-38	{2110;001;20;0}	$8q^{18}$
5-17	{1122;210;00;0}	$8q^{17}$	5-39	{0210;102;00;0}	$32q^{20}$
5-18	{1110;220;02;0}	$8q^{17}+8q^{18}$	5-40	{2102;010;00;0}	$16q^{19}$
5-19	{1110;222;00;0}	$8q^{17}$	5-41	{0102;012;00;0}	$4q^{18}+12q^{19}+8q^{20}$
5-20	{2112;110;20;0}	$4q^{16}$	5-42	{0220;202;00;0}	$4q^{21}+16q^{22}+12q^{23}+2q^{24}$
5-21	{1100;020;02;0}	$8q^{20}$	5-43	{2022;200;00;0}	$8q^{21}+12q^{22}$
5-22	{1100;022;00;0}	$4q^{19}$	5-44	{0222;220;00;0}	$8q^{20}$
			5-45	{2222;000;00;0}	q^{20}

TABLE II: Bond lists and perimeter polynomials, $D_c(q)$, for the quintet types ($n_c=5$) of the J_1 - J_2 model. The labels for the cluster types are as in Fig. 2.

hand, the same pure J_1 cluster type, with the exception of cluster type 2-1, has several configurations. For example, cluster type 3 in Fig. 3 of I has two configurations in the J_1 model (configurations 3α and 3β in Fig. 4 of I). The same cluster type exists in the J_1 - J_2 model as cluster type 3-1 (Fig. 1 of the present paper), but the only configuration is 3α , with the two J_1 bonds at 180° angle.

Similar results are obtained for the pure cluster types in the J_1 - J_3 model: 1) The pure J_3 cluster types of this model, together with the single, are identical to the 10 cluster types of the parent J_3 model. 2) The pure J_1 cluster types, together with the single, are only a subset of the cluster types of the parent J_1 model. In this case, the reason why they are only a subset is that in the J_1 - J_3 model any configuration that has two consecutive J_1 bonds at 180° angle, also has at least one J_3 bond. Therefore, in the J_1 - J_3 model it is a configuration of a mixed cluster, not of a pure J_1 cluster. If all configurations of a particular cluster type c of the J_1 model contain consecutive J_1 bonds that make 180° angle, then this cluster type is not among the pure J_1 cluster types of the J_1 - J_3 model.

To follow up on the previous example of cluster type 3 in Fig. 3 of I, this cluster type is identical to cluster type 3-2 in the J_1 - J_3 model (Fig. 3 of the present paper),

which is a pure- J_1 cluster type. Cluster type 3-2 of the J_1 - J_3 model has only one configuration, namely, the 3β configuration in which the two consecutive J_1 bonds are at 90° angle.

APPENDIX D: COMMENTS ON THE PROBABILITIES OF PURE CLUSTER TYPES IN THE J_1 - J_2 AND J_1 - J_3 MODELS

As discussed in Appendix C, the pure J_2 cluster types of the J_1 - J_2 model are identical to cluster types of the parent J_2 model. The configurations for each of these cluster types are also the same in the two models. However, the probability P_c for each of these cluster types is lower in the J_1 - J_2 model than in the J_2 model. The reason is that the J_1 - J_2 perimeter for any configuration is larger than the J_2 perimeter for the same configuration (see Sec. II C). Similar remarks also apply to the probabilities for the pure J_3 cluster types in the J_1 - J_3 model, compared to the probabilities for the same cluster types in the parent J_3 model.

The case of the pure J_1 cluster types is somewhat different. Each of the pure J_1 cluster types in the J_1 - J_2 model is identical to one of the cluster types in the par-

Cluster type, c	Bond List	$D_c(q)$
1-1	{}	q^8
2-1	{1}	$2q^{12}$
2-2	{3}	$2q^{13}$
3-1	{11;3}	$2q^{16}$
3-2	{11;0}	$4q^{15}$
3-3	{13;0}	$8q^{16}+4q^{17}$
3-4	{33;0}	$4q^{17}+2q^{18}$
4-1	{113;31;0}	$2q^{20}$
4-2	{131;10;0}	$8q^{18}$
4-3	{110;01;0}	$4q^{18}$
4-4	{111;30;0}	$4q^{18}$
4-5	{011;11;0}	q^{16}
4-6	{110;33;0}	$8q^{19}+4q^{21}$
4-7	{113;30;0}	$4q^{19}$
4-8	{110;03;0}	$16q^{19}+8q^{20}$
4-9	{113;00;0}	$8q^{19}$
4-10	{130;03;0}	$4q^{20}+8q^{21}+2q^{22}$
4-11	{130;00;3}	$16q^{20}+16q^{21}+4q^{22}$
4-12	{133;00;0}	$12q^{20}$
4-13	{130;03;1}	$2q^{18}$
4-14	{310;01;0}	$4q^{19}+8q^{20}+2q^{21}$
4-15	{330;03;0}	$4q^{21}+8q^{22}+2q^{23}$
4-16	{333;00;0}	$4q^{21}$
4-17	{033;33;0}	q^{20}

TABLE III: Bond lists and perimeter polynomials, $D_c(q)$, for cluster types of the J_1 - J_3 model that have sizes $1 \leq n_c \leq 4$. The labels for the cluster types are as in Fig. 3.

ent J_1 model. However, the probability P_c is lower in the J_1 - J_2 model, for two reasons. One is that, with the exception of cluster type 2-1, the number of configurations in the J_1 - J_2 model is smaller than in the parent J_1 model (see Appendix C). The second reason is that for those configurations that exist in both models, the J_1 - J_2 perimeter is larger than the J_1 perimeter. A larger perimeter implies a lower probability for the configuration. For the same two reasons the probability P_c for any pure J_1 cluster types in the J_1 - J_3 model is lower than that for the same cluster type in the J_1 model.

* Electronic address: yshapira@granite.tufts.edu

† Electronic address: vbindilatti@if.usp.br

¹ V. Bindilatti and Y. Shapira, Phys. Rev. B **72**, 064414 (2005), URL <http://link.aps.org/abstract/PRB/v72/e064414>.

² Y. Shapira and V. Bindilatti, J. Appl. Phys. **92**, 4155 (2002), URL <http://link.aip.org/link/?jap/92/4155>.

³ T. Q. Vu, V. Bindilatti, Y. Shapira, E. J. McNiff, Jr., C. C. Agosta, J. Papp, R. Kershaw, K. Dwight, and A. Wold, Phys. Rev. B **46**, 11617 (1992), URL <http://publish.aps.org/abstract/PRB/v46/p11617>.

⁴ V. Bindilatti, E. ter Haar, N. F. Oliveira, Jr., Y. Shapira, and M. T. Liu, Phys. Rev. Lett. **80**, 5425 (1998), URL <http://publish.aps.org/abstract/PRL/v80/p5425>.

⁵ V. Bindilatti, E. ter Haar, N. F. Oliveira, Jr., Y. Shapira, and M. T. Liu, J. Appl. Phys. **85**, 5950 (1999), URL <http://link.aip.org/link/?jap/85/5950>.

⁶ D. Stauffer and A. Aharony, *Introduction to Percolation Theory, Revised* (Taylor & Francis, London, 1994), revised 2nd ed.

⁷ Y. Shapira and V. Bindilatti, arXiv:cond-mat/0609715 (2006), <http://arxiv.org/abs/cond-mat/0609715>.

⁸ A “realization” of a cluster type is any one cluster of this

type. Similarly, a realization of a configuration is any one set of cation sites arranged in this configuration.

⁹ K. Malarz and S. Galam, Phys. Rev. E **71**, 016125 (2005), URL <http://link.aps.org/abstract/PRE/v71/e016125>.

In addition to percolation concentrations, this work also discusses some symmetry properties of neighbors on the square lattice.

¹⁰ H. P. Peters, D. Stauffer, H. P. Holters, and K. Loewenich, Z. Physik B - Condensed Matter **34** (1979).

¹¹ To avoid infinite values in the derivative, dM/dB was evaluated at a very low, but non-zero, temperature T .

¹² Including the derivative of $R(T, B)$ can lead to an error if $R(T, B)$ is obtained by the CQUIN’s method. In this method the true clusters with $n_c > 5$ are replaced by fictitious quintets. Including the derivative of $R(T, B)$ in the spectrum would lead to an artificial enhancement of spectral lines from quintets.

¹³ X. Gratens and *et al.*, to be published (2006).

¹⁴ In the range $J_2/J_1 \leq 1$ the positions of the five spectral lines from the 3-1 triplets remain exactly at $b_1 = 7, 9, 11, 13$ and 15. In the same range of J_2/J_1 the 3-2 triplets produce lines at exactly the same fields, so that all the 3-1 lines coincide with 3-2 lines. However, when $\frac{1}{2} \leq J_2/J_1 \leq 1$, the

Cluster Type, c	Bond List	$D_c(q)$	c	Bond List	$D_c(q)$
5-1	{1133;310;01;0}	$2q^{24}$	5-30	{1130;303;00;0}	$8q^{22}+8q^{24}$
5-2	{1310;130;01;0}	$8q^{22}$	5-31	{1133;300;00;0}	$2q^{22}$
5-3	{1130;010;01;0}	$8q^{21}$	5-32	{1100;030;00;3}	$8q^{22}+24q^{23}+32q^{24}+8q^{25}$
5-4	{1133;010;01;0}	$4q^{20}$	5-33	{1100;030;03;0}	$4q^{22}+20q^{23}+8q^{24}+4q^{25}$
5-5	{0110;101;00;0}	$4q^{20}$	5-34	{1100;033;00;0}	$24q^{23}$
5-6	{3110;101;00;3}	$4q^{20}$	5-35	{1130;000;00;3}	$16q^{23}+8q^{24}$
5-7	{3110;101;00;0}	$4q^{20}$	5-36	{1130;003;00;0}	$24q^{23}+16q^{24}$
5-8	{1131;310;00;0}	$8q^{21}$	5-37	{1133;000;00;0}	$4q^{22}$
5-9	{1311;100;00;3}	$4q^{20}$	5-38	{1300;000;30;3}	$16q^{24}+40q^{25}+24q^{26}+4q^{27}$
5-10	{1110;301;00;0}	$8q^{20}$	5-39	{1300;000;33;0}	$24q^{24}+12q^{25}$
5-11	{1101;013;10;0}	$8q^{19}$	5-40	{1300;003;30;0}	$32q^{24}+24q^{25}+24q^{26}+4q^{27}$
5-12	{1111;300;00;3}	q^{20}	5-41	{1033;300;00;0}	$8q^{24}+12q^{25}$
5-13	{1130;310;03;0}	$8q^{23}+4q^{25}$	5-42	{1330;000;03;0}	$32q^{24}+24q^{25}$
5-14	{1133;310;00;0}	$8q^{22}$	5-43	{1333;000;00;0}	$4q^{23}$
5-15	{1310;100;03;0}	$16q^{21}+8q^{23}$	5-44	{1033;000;33;0}	$8q^{23}$
5-16	{1130;010;03;0}	$8q^{22}+8q^{23}$	5-45	{1100;330;00;1}	$8q^{22}+8q^{23}+8q^{24}+4q^{25}$
5-17	{1103;310;00;0}	$16q^{21}$	5-46	{3110;001;30;0}	$4q^{23}$
5-18	{1313;100;00;0}	$8q^{21}+8q^{22}$	5-47	{1130;303;00;1}	$8q^{21}$
5-19	{1100;010;03;0}	$8q^{21}+8q^{22}+8q^{23}$	5-48	{1010;300;01;0}	$8q^{21}+24q^{22}+16q^{23}+8q^{24}$
5-20	{1103;010;00;0}	$16q^{22}$	5-49	{3011;100;00;0}	$8q^{22}+8q^{23}$
5-21	{1110;303;00;0}	$16q^{21}+8q^{23}$	5-50	{1301;030;10;0}	$8q^{21}$
5-22	{1110;003;30;0}	$8q^{22}+4q^{23}$	5-51	{0103;013;00;0}	$4q^{22}+20q^{23}+16q^{24}+12q^{25}+2q^{26}$
5-23	{1113;300;00;0}	$4q^{21}$	5-52	{0310;103;00;0}	$8q^{23}+32q^{24}+24q^{25}+4q^{26}$
5-24	{0113;110;00;0}	$8q^{20}$	5-53	{1303;030;10;0}	$16q^{22}$
5-25	{1100;330;03;0}	$4q^{22}+8q^{24}+2q^{26}$	5-54	{3103;010;00;0}	$32q^{23}+24q^{24}$
5-26	{1100;330;00;3}	$8q^{23}+8q^{24}+8q^{25}+4q^{26}$	5-55	{0330;303;00;0}	$4q^{25}+16q^{26}+12q^{27}+2q^{28}$
5-27	{1100;333;00;0}	$4q^{22}+8q^{23}$	5-56	{3033;300;00;0}	$8q^{25}+12q^{26}$
5-28	{1100;330;03;3}	$4q^{22}$	5-57	{0333;330;00;0}	$8q^{24}$
5-29	{1130;300;00;3}	$8q^{23}+4q^{24}$	5-58	{3333;000;00;0}	q^{24}

TABLE IV: Bond lists and perimeter polynomials, $D_c(q)$, for quintet types ($n_c=5$) of the J_1 - J_3 model. The labels for the cluster types are as in Fig. 4.

3-2 triplets produce additional lines at $b_1 < 7$. The values of b_1 at these additional lines depend on the ratio J_2/J_1 .

¹⁵ Conclusions based on numerical simulations for specific values of S and specific ratios J_2/J_1 fall short of being proven. However, the physical arguments in the following paper give strong additional support to these conclusions.

¹⁶ All lattice sites of the square lattice in Fig. 1 of I can be reached from the central site by successive jumps between NN sites. The sublattice consisting of all sites that can be reached from the central site by successive jumps between 2nd neighbors is, by itself, also a square lattice. Compared to the original square lattice, this “new” square lattice has a lattice constant that is a factor of $\sqrt{2}$ larger, and it is rotated by 45° . The J_2 exchange bonds in the original square lattice are the NN exchange bonds in the new square lattice. All configurations, cluster types, clus-

ter Hamiltonians, and cluster statistics for the original J_2 model are identical to those of the “ J_1 model” for the new square lattice. A similar argument applies to the sublattice consisting of all sites that can be reached from the central site by successive jumps between 3rd neighbors.

¹⁷ In a given material the numerical value of J is specified by the symmetry class of the neighbor associated with J , i.e., it depends on whether J is J_1 , or J_2 , or J_3 . However, if the material is not specified then the numerical value of J is not known even if the symmetry class is known. In that case, J is just a parameter in the exchange Hamiltonian. As long as it remains just a parameter, there is no difference between the exchange Hamiltonians of isomorphic cluster types.